

A graph-based approach to glacier flowline extraction: an application to glaciers in Switzerland

Nicolas Le Moine^{a,*}, Pierre-Stéphane Gsell^a

^a*Sorbonne Universités, UPMC Univ. Paris 06, CNRS, EPHE, UMR Metis*

Abstract

In this paper we propose a new, graph-based approach to glacier segmentation and flowline extraction. The method, which requires a set of glacier contours and a Digital Elevation Model (DEM), consists in finding an optimum branching that connects a set of vertices belonging to the topological skeleton of each glacier. First, the challenges associated with glacier flowline extraction are presented. Then, the three main steps of the method are described: the skeleton extraction and pruning algorithm, the definition and computation of a travel cost between all pairs of skeleton vertices, and the identification of the directed minimum spanning tree in the resulting directed graph. The method, which is mainly designed for valley glaciers, is applied to glaciers in Switzerland.

Keywords: glacier flowline, skeleton, discrete curve evolution, optimum branching, directed minimum spanning tree

1. Introduction

1.1. Glacier morphology

Glaciers are moving ice bodies which flow under their own weight, due to the accumulation of solid precipitations on the higher slopes of a mountain range. As the strain rate increases, ice viscosity decreases and the accumulated ice literally ‘flows’ downslope. Bahr and Peckham (1996) first explicitly drew a parallel between rivers and valley glaciers (i.e. glaciers that are confined by topography, as opposed to ice caps). They showed that glaciers also

*Corresponding author

Email address: `nicolas.le_moine@upmc.fr` (Nicolas Le Moine)

exhibit branching topologies, and computed classical river network indices such as bifurcation and area ratios for glacier networks. This analogy stems from the fact that in most recent orogens where valley glaciers are found (the Alps, the Andes, the Himalayas, the Rocky Mountains, etc.), glacier inception took place in a topography previously shaped by fluvial erosion (Gsell et al., 2014). Bahr and Peckham also pointed out that self-similarity properties could provide a ‘lever arm’ for tackling glacier flow dynamics for complex geometries, just as these properties are used for treating subgrid, hydraulic propagation in complex river networks with concepts such as the Geomorphological Instantaneous Unit Hydrograph (Rodríguez-Iturbe and Valdés, 1979; Gupta et al., 1980). One of the reasons why this approach has not been given much attention is maybe the difficulty lying in the first step of identifying networks of glacier flowlines.

1.2. Limits of classical drainage network extraction methods

Figure 1 shows the downstream region of the Rhone glacier in Switzerland. In fluvial morphology, we typically find cross-sections such as A–A’ with a concave topography in the talweg. This translates into V- or U-shaped (for former glacial valleys) elevation contours, with the lowest point roughly in the medial axis of the talweg. Hence, river network extraction from a DEM is relatively straightforward, except for problems such as flat areas or closed depressions (see e.g. Garbrecht and Martz, 1997; Martz and Garbrecht, 1998).

Things are more complicated for ice-covered areas. In the accumulation (higher) area of the glacier, where hillslopes as well as valley floors are ice-covered, the topography is still concave (B–B’): the surface of the ice is more or less homothetic to the bedrock surface (with lower roughness though). In contrary, in the ablation area the glacier is limited to a narrow ice tongue confined between lateral, ice-free hillslopes. Since ice thickness is maximum in the medial axis of the ice tongue, we have a convex cross-section (C–C’) with seemingly two talwegs on each side of the glacier. Elevation contours in this area have the shape of a W with its two wedges pointing upstream, as opposed to the single wedge in concave topography. The central flowline of the glacier (i.e. the line of maximum ice thickness), which is also typically the line of the bedrock talweg, is a local maximum and not a local minimum of the ice surface (it looks like is a local water divide). Therefore, it cannot be extracted in a stable way from a DEM with classical algorithms.

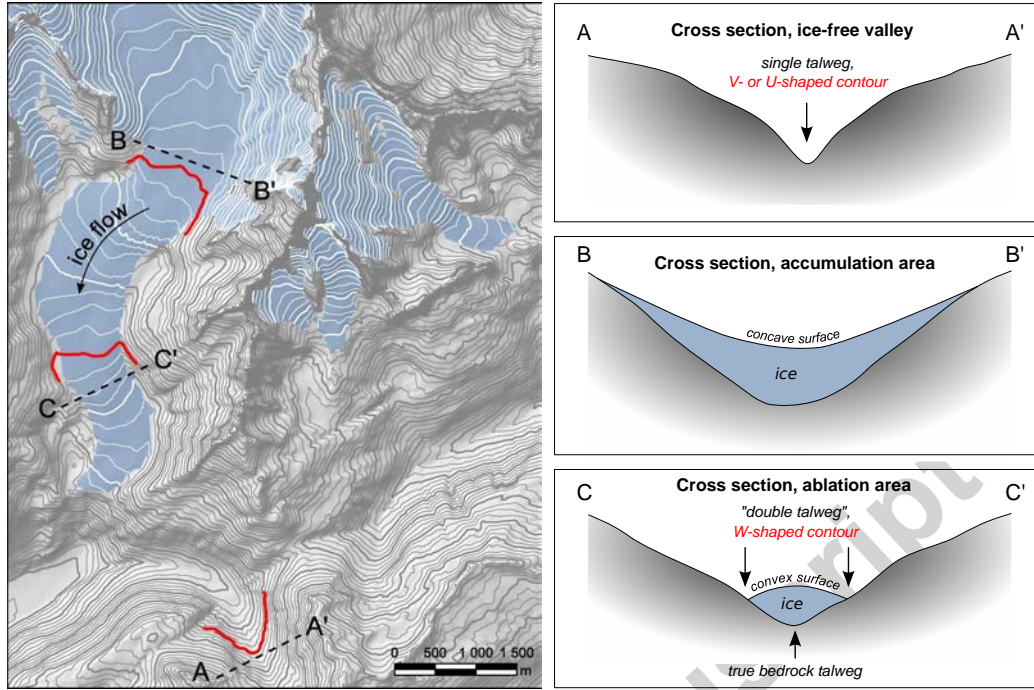


Figure 1: Illustration of the spurious ‘double talweg’ in glacial landscape. This feature mainly appears in the glacier’s ablation area where a narrow ice tongue is confined in a valley (C–C’). On a map, elevation contours in this area have the shape of a W with its two wedges pointing upstream, whereas contours in classical (ice-free) valleys are V- or U-shaped with a single wedge pointing upstream (A–A’).

1.3. Automatic methods for glacier flowline extraction

The problem of glacier flowline extraction has received some attention recently, due to the need of feeding glacier databases with attributes such as glacier length. A flowline or a set of flowlines has to essentially meet two requirements: (i) to stay as far as possible from the glacier boundary, and (ii) to cross elevation contours orthogonally. Le Bris and Paul (2013) propose to construct a set of waypoints located at the center of ‘traverses’ drawn perpendicular to a single, rectilinear ‘main axis’, and then connect them. However, the method can only extract one centerline per glacier. Kienholz et al. (2014) use a more complex approach based on a cost function which quantifies the trade-off between the two requirements; a set of flowlines is then extracted between glacier heads and a single snout (terminus) per glacier. Other methods apply alternate procedures in the accumulation and

ablation zones (Machguth and Huss, 2014), also resulting in a large number of parameters.

1.4. Objectives of the study

In this paper, a new method is presented that aims at extracting glacier flowlines with an emphasis on preserving their tree-like structure, i.e. the structure of tributaries within the glacier.

As in Le Bris and Paul (2013), our method first identifies a set of waypoints (i.e., vertices of a graph) that are subsequently connected. However these waypoints are identified with a more general operation called skeletonization. Once these waypoints are identified (including special ‘snout’ vertices), we compute a travel cost between every pair of them: the cost function is designed so as to penalize displacements that deviate from the steepest slope direction. The main difference with Kienholz et al. (2014) is the formulation of an anisotropic cost function. The final step is to construct a directed minimum spanning tree (DMST) that allows to visit all waypoints at minimal cost, starting from a snout (root) vertex. Edges of this DMST meet the two requirements: they stay ‘far’ from the glacier’s boundary (since they link waypoints belonging to the skeleton), and they deviate little from the steepest slope direction since they are least-cost paths with respect to the slope-dependent cost function. The overall procedure requires only 5 parameters, in contrast with other methods (e.g. 16 parameters in Kienholz et al., 2014 and 17 in Machguth and Huss, 2014).

The method is mainly designed for valley glaciers, as ice caps usually do not exhibit strong branching topologies. It is tested on a dataset of Swiss glaciers (Figure 2a), covering a total area of 1200 km² and mainly located in the headwaters of the Rhone, Rhine, and Danube rivers. The steps of the method are illustrated with a focus on a particular glacier complex in the Bernese Alps (Figure 2b), straddling the water divide between the Rhone and Rhine rivers.

2. Data

2.1. Digital Elevation Model

In this study we use the 25-meter Digital Elevation Model from the Swiss Federal Office of Topography (SwissTopo, 2004).

2.2. *Randolph Glacier Inventory (RGI) glacier contours*

Glacier outlines are taken from the Randolph Glacier Inventory (RGI, Arendt et al., 2012). The RGI provides a segmentation of glacier complexes (continuous ice bodies) into individual glaciers; we chose to dissolve (re-aggregate) these elements and to work with the complexes in order test the ability of our approach to identify multiple snouts in such complexes. The segmentation is not a prerequisite and is even a by-product of our method.

3. **Skeleton extraction and pruning**

3.1. *Glacier flowlines as a topological skeleton*

The method proposed by Le Bris et al. (2013), which consists in picking the midpoints of ‘traverses’ drawn orthogonally to the glacier’s ‘main axis’, is actually related to a topological operation called skeletonization, or medial-axis transform. A first, intuitive definition is the analogy with a grassfire (Blum, 1967): if one ‘sets fire’ simultaneously at all points on the border of a grass field enclosed in the object’s boundary, then the skeleton is the set of points where two or more firefronts meet (see Figure 3a). The result (Figure 3b) is a ‘thinned’ version of the object (i.e., a set of edges, namely a graph) that preserves its essential geometrical and topological features (in the example of Figure 3, the skeleton edges look like the veins of the leaf). We will see that this is a first interesting step to glacier flowline extraction.

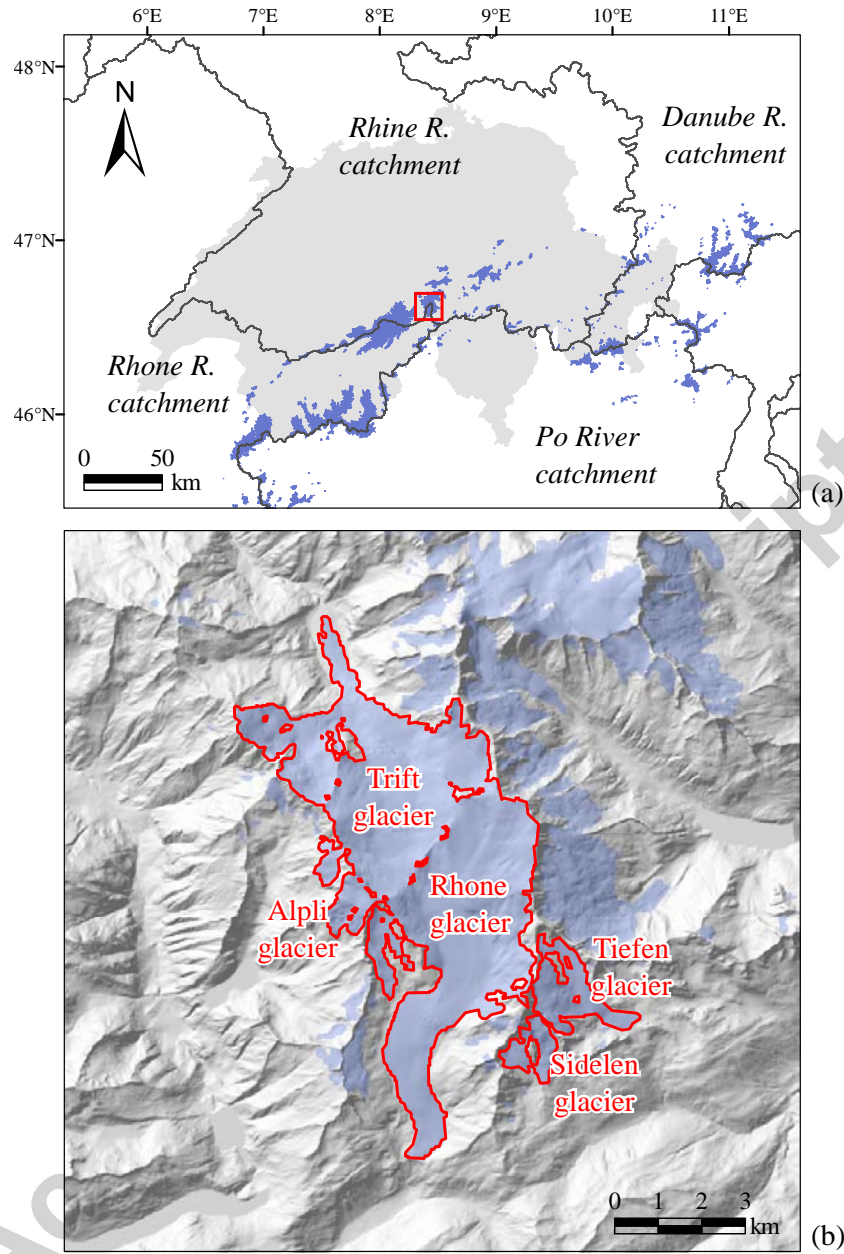


Figure 2: Area covered by this study. (a) Map of Switzerland with glacier contours in dark blue. (b) Zoom on the Rhone-Trift glacier complex illustrating the steps throughout the paper. This complex covers 35.8 km^2 and includes two large glaciers: the Rhone glacier (15.9 km^2) and the Trift glacier (16.6 km^2) as well as a number of smaller ones (e.g. Tiefen, Sidelen and Alpli glaciers).

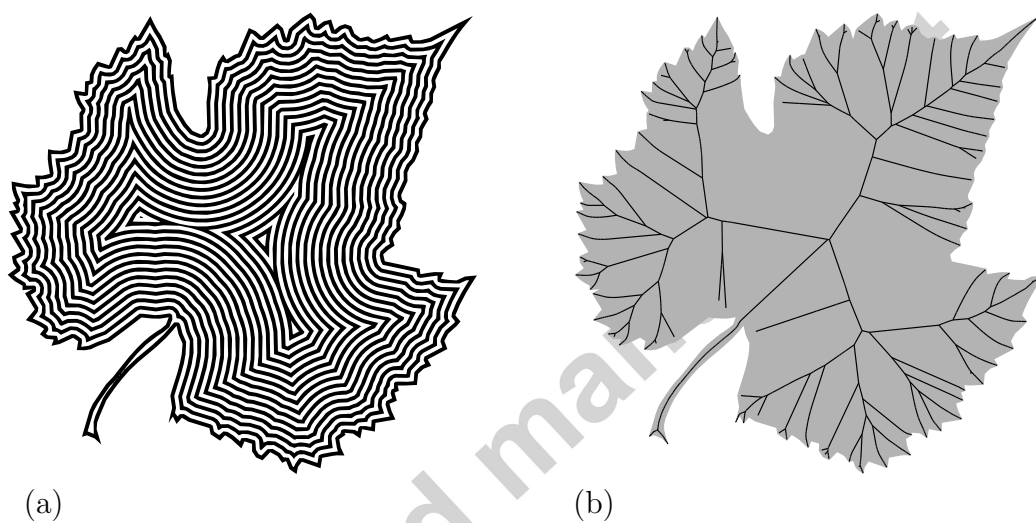


Figure 3: Grassfire analogy of the skeletonization: (a) propagation of the 'firefronts'; (b) resulting skeleton i.e. the set of points where two or more fronts meet.

114 3.2. Skeletonization using Voronoi tessellation

115 A second definition of the skeleton uses the concept of maximal disk (or
116 maximal ball in dimensions higher than 2). A disk \mathcal{B} is said to be maximal
117 in set \mathcal{D} if it is completely included in \mathcal{D} , and such that if it is contained in
118 any other disc \mathcal{B}' then \mathcal{B}' is not completely included in \mathcal{D} . Mathematically,

$$\mathcal{B} \text{ is a maximal disk in set } \mathcal{D} \text{ iff } \begin{cases} \mathcal{B} \subseteq \mathcal{D} \\ \mathcal{B} \subset \mathcal{B}' \Rightarrow \mathcal{B}' \not\subseteq \mathcal{D} \end{cases} \quad (1)$$

119 A maximal disk $\mathcal{B}(\mathbf{s})$ centered at point \mathbf{s} is entirely contained in \mathcal{D} and is
120 interiorly tangent to the boundary $\partial\mathcal{D}$ in at least two different points, called
121 generating points: these are two locations where firefronts originate from in
122 the grassfire analogy, and they meet at the center of a maximal disk. The
123 skeleton $S(\mathcal{D})$ can be defined as the set of the centers of all maximal disks
124 in \mathcal{D} :

$$S(\mathcal{D}) = \{\mathbf{s} \mid \mathcal{B}(\mathbf{s}) \text{ is a maximal disk in } \mathcal{D}\} \quad (2)$$

125 Figure 4 illustrates this definition. $Gen(\mathbf{s}) \subset \partial\mathcal{D}$ denotes the generating
126 points of the skeletal point $\mathbf{s} \in S(\mathcal{D})$.

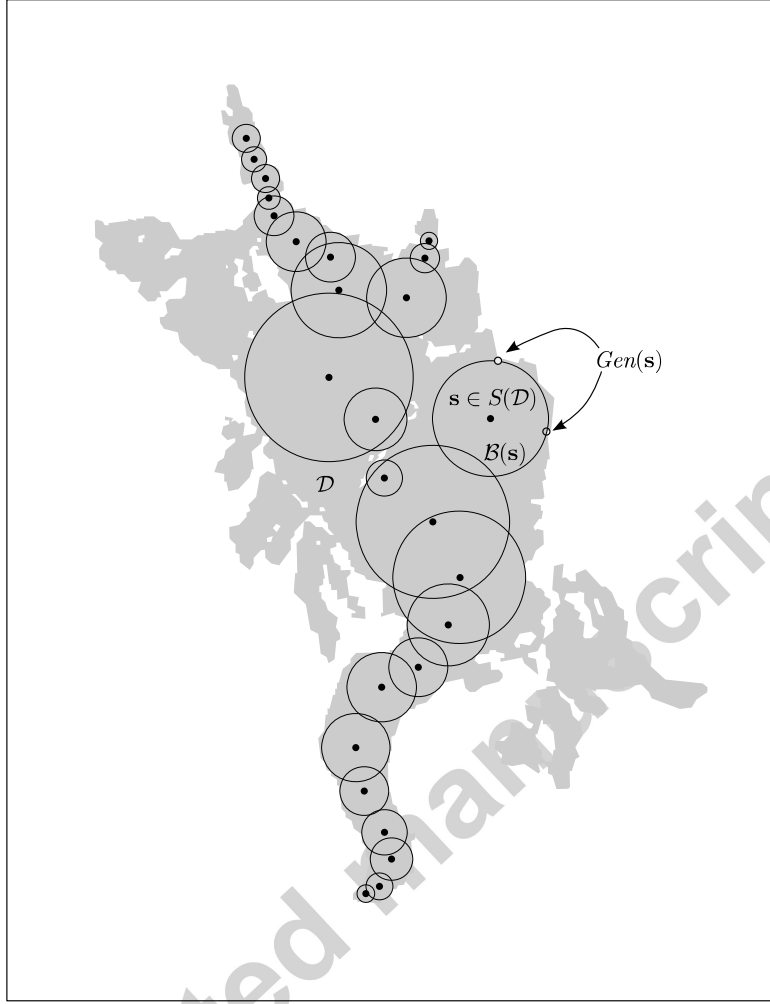


Figure 4: Definition of skeleton $S(\mathcal{D})$ as the set of centers of all maximal disks in \mathcal{D} (gray shape). $Gen(s)$ denotes the generating points of the skeletal point s .

One possibility to generate the skeleton is to implement a ‘grassfire’ algorithm. Given the previous definition, another method uses the Voronoi tessellation (see e.g. Brandt and Algazi, 1992) of a set of points (input sites) sampled along the boundary (see Figure 5). Each Voronoi region represents the area closest to a boundary input site, and is delimited by several edges: hence, each edge \mathcal{E} is a segment of the perpendicular bisector of a *pair* of input sites. To show the similarity with the previous results, we call this pair the generating pair $Gen(\mathcal{E})$ of the edge. As the number n of input sites sam-

135 pled on the boundary increases ($n \rightarrow \infty$), the set of edges of the tessellation
 136 that are contained in the domain \mathcal{D} converges to the exact skeleton.



Figure 5: Skeletonization using the Voronoi tessellation of a set of boundary input sites. The set of internal edges of the tessellation (solid black lines) converges to the skeleton as the number of points on the boundary increases (left: one point every 2000 m ; right: one point every 500 m).

137 We used the Qhull library (Barber et al., 1996) to generate the tesse-
 138 lation. It allows to retrieve not only the Voronoi edges but also the pair
 139 of generating input sites (boundary points) for each edge, a highly valuable
 140 information for the subsequent steps. It is worth noting that the object may
 141 have inner boundaries (‘holes’ in the shape, such as inner rocks for a glacier),
 142 which will translate into cycles in the skeletal graph.

143
 144 RGI glacier contours were first densified so as to have at least one point
 145 every 50 m along the boundary, before running the tessellation with Qvoronoi.
 146 All subsequent steps were then performed under Scilab (Scilab Entreprises,
 147 2012), using the CLaRiNet library (Le Moine, 2013).

3.3. Skeleton pruning through Discrete Curve Evolution

As mentioned previously, the set of edges obtained with the Voronoi tessellation is only an approximation of the skeleton. Moreover, due to the noise in the boundaries, insignificant boundary features can generate skeleton edges which do not reflect essential topological properties. Hence, we need to simplify, or ‘prune’, the skeleton i.e. remove many spurious edges.

In this study we use the pruning algorithm of Bai et al. (2007), who point out that not all n boundary points significantly contribute to the shape of the object: only a relatively small subset of these boundary (input) sites may be sufficient to describe the overall shape. Hence, if we select $k \leq n$ points on the boundary, we define a partition of the contour into k contour segments (subarcs). The pruning rule is to remove all skeleton edges whose generating points lie on a same contour segment, as illustrated in Figure 6. It is important to note that this pruning process is not equivalent to reducing the number of input sites in the Voronoi tessellation (i.e. moving from right to left in Figure 5): the pruning removes some edges but the geometry of the remaining ones is not altered.

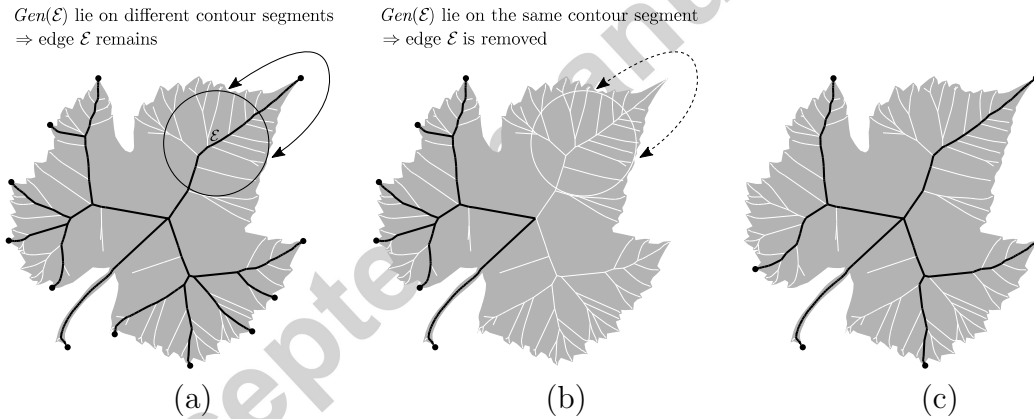


Figure 6: Pruning of the skeleton based on contour partitioning. Skeleton edges which have their generating points lying on a same contour segment are removed (in white). (a) Partition with $k = 12$ points; (b) $k = 6$ points; (c) $k = 6$ points but at different locations.

The problem is to select the k most relevant points; Bai et al. (2007) propose to reduce the number of boundary points from n to $k < n$ through Discrete Curve Evolution (DCE).

Let $\mathbf{c}_1, \dots, \mathbf{c}_n$ be the n input sites sampled on the boundary, and let $\mathbf{u}_{i-1,i} = \mathbf{c}_i - \mathbf{c}_{i-1}$ and $\mathbf{u}_{i,i+1} = \mathbf{c}_{i+1} - \mathbf{c}_i$ be the vectors of the boundary edges incident to point \mathbf{c}_i (Figure 7). The contribution of this site to the overall shape is (Latecki and Lakämper, 2002):

$$K(\mathbf{c}_i) = \frac{\theta_i \|\mathbf{u}_{i-1,i}\| \|\mathbf{u}_{i,i+1}\|}{\|\mathbf{u}_{i-1,i}\| + \|\mathbf{u}_{i,i+1}\|} \quad (3)$$

where

$$\theta_i = (\widehat{\mathbf{u}_{i-1,i}, \mathbf{u}_{i,i+1}}) = \arccos\left(\frac{\mathbf{u}_{i-1,i} \cdot \mathbf{u}_{i,i+1}}{\|\mathbf{u}_{i-1,i}\| \|\mathbf{u}_{i,i+1}\|}\right) \text{sgn}(\det(\mathbf{u}_{i-1,i}, \mathbf{u}_{i,i+1}))$$

is the oriented turn angle at point \mathbf{c}_i (trigonometric, i.e. measured counter-clockwise). This contribution is usually defined in 2D (planar computation), but there is no difficulty in extending it to a 3D curve. However, even if glaciers are located on steep topography, they remain objects in the geographical space i.e. with a rather flat aspect ratio, so that the addition of the vectors' z-coordinate would not change the contributions dramatically.

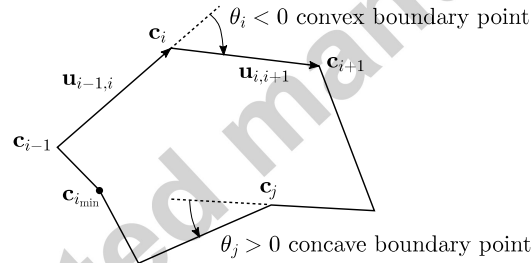


Figure 7: Definition of the turn angle at a boundary point.

Since contours are closed, we set $\mathbf{c}_{n+1} = \mathbf{c}_1$ and $\mathbf{c}_0 = \mathbf{c}_n$. If boundary points are sorted clockwise (i.e. with the ‘inside’ on the right and the ‘outside’ on the left when moving along the boundary, as in the ESRI[®] shapefile format), then:

- K is negative for a convex point (clockwise turn), and positive for a concave point (counterclockwise turn),
- the higher the absolute value $|K|$, the higher the contribution to the overall shape (through great segment lengths and/or large turn angle).

188 A point lying on a straight contour portion, i.e. such that $\theta = 0$, will
 189 have a zero contribution (i.e. it can be removed without any loss of
 190 shape information).

191 We start the DCE with the n initial input sites and we removes the point
 192 $\mathbf{c}_{i_{\min}}$ having the lowest absolute value $|K(\mathbf{c}_{i_{\min}})|$, thus leading to a simplified
 193 contour called DCE level $n-1$. The metric K is again computed for the $n-1$
 194 remaining points, and the procedure is repeated p times to obtain a hierar-
 195 chical set of contour partitions, called DCE level $n-2, n-3, \dots, k = n-p$.
 196 At each iteration, we remove the skeleton edges whose generating points lie
 197 on a same contour segment of DCE level $k = n-p$, and these edges are
 198 assigned the level k . Since we need at least two points on the contour to
 199 define a partition, the highest possible level is $k = 2$. Figure 6c actually rep-
 200 resents DCE level 6 of the leaf, and in Figure 8 we show the final hierarchy
 201 of skeleton edges.

202
 203 If the shape has one or several inner boundaries, we simply add a loop on
 204 the boundaries in order to find the least-contributing site at each iteration.



Figure 8: Hierarchy of skeleton edges obtained at the end of the pruning algorithm: we can stop at any level in this hierarchy.

205 4. Identification of snout vertices

206 In the previous section we illustrated the skeleton extraction and pruning
 207 with a simple shape (a leaf); we now apply these methods to RGI contours

of Swiss glaciers. The main issues will be to decide the level k at which we should extract the skeleton for each glacier, and to use elevation data in order to identify snout and head vertices.

4.1. Choice of DCE level for each glacier

Consider a glacier with area A . Clearly, the larger the glacier, the more points will be needed on its boundary to correctly describe its shape or skeleton, i.e. the higher we will need to stay in the DCE hierarchy. Conversely, a small glacier with a single main axis without tributary could be correctly described at DCE level $k = 2$. A selection rule of thumb $k = f(A)$ was devised empirically upon visual appreciation:

$$(k - 2) = \lfloor k_0 A^\gamma \rfloor$$

where $\lfloor \cdot \rfloor$ is the floor function. We used $k_0 = 13.5$ and $\gamma = 0.8$ with A in km^2 . For example, the skeleton of Rhone-Trift glacier complex, with an area $A = 35.8 \text{ km}^2$, is still correctly described at DCE level $k = 2 + 13.5(35.8)^{0.8} = 238$, i.e. with 238 sites on its boundary (Figure 9, left panel).

4.2. Hierarchical snout identification

The next step is the orientation of the skeletal edges in order to identify glacier snouts and heads. Indeed, skeletonization is a planar operation and we do not know if a ‘leaf’ vertex in the skeleton corresponds to the beginning of a flowline (‘head’ vertex), or to its end (‘snout’ vertex). Again, we will use the results of the DCE algorithm to create a hierarchy of potential snouts. A skeletal vertex \mathbf{s} is said to be a level- k snout if it meets the three following requirements:

- (i) \mathbf{s} is a leaf vertex of the skeletal graph of DCE level k , i.e. having a degree (number of incident edges) $d = 1$,
- (ii) \mathbf{s} is at an elevation lower than its closest vertex \mathbf{s}' of degree $d \neq 2$ in the level k skeleton graph. \mathbf{s}' is such that all vertices on the path between \mathbf{s} and \mathbf{s}' have degree 2: in the following we will call such a sequence of vertices of degree 2 (except the two extremal vertices) a *stretch*.
- (iii) the generating points $Gen(\mathcal{E}_{\mathbf{s}})$ of its unique incident edge $\mathcal{E}_{\mathbf{s}}$ (pendant edge) lie on either side of an input site which is a local topographic minimum in the DCE level k .

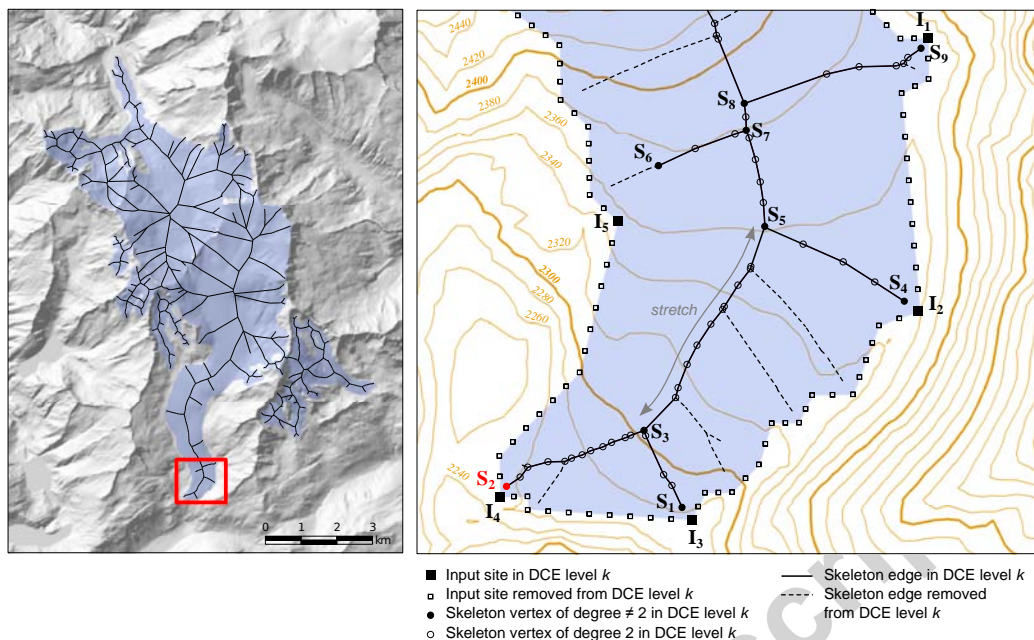


Figure 9: Definition of a snout vertex in the skeleton pruned at DCE level k ($k = 238$ here).

239 These seemingly complicated requirements translate the more intuitive
240 notion that an edge is at a snout if it points downslope in a locally convex
241 portion of the boundary that also points downslope, as shown in Figure 9.

On Figure 9, skeleton edges at level k are drawn in solid black lines, while edges that have been pruned at earlier levels are drawn with dotted lines. There are several ‘candidate’ snouts in this area: skeleton vertices \mathbf{S}_1 , \mathbf{S}_2 , \mathbf{S}_4 , \mathbf{S}_6 and \mathbf{S}_9 , which are all leaf vertices at the current pruning level, i.e. meeting requirement (i). All these 5 vertices also satisfy requirement (ii), since we have:

$$\begin{array}{ll}
 \text{Leaf vertex} & \text{Nearest vertex of degree } \neq 2 \\
 z(\mathbf{S}_1) & < z(\mathbf{S}_3) \\
 z(\mathbf{S}_2) & < z(\mathbf{S}_3) \\
 z(\mathbf{S}_4) & < z(\mathbf{S}_5) \\
 z(\mathbf{S}_6) & < z(\mathbf{S}_7) \\
 z(\mathbf{S}_9) & < z(\mathbf{S}_8)
 \end{array}$$

However, Table 1 shows that only one candidate satisfies the third requirement:

Leaf vertex	Input site in DCE level k that separates the vertex’s generating pair	Is requirement (iii) met ?
\mathbf{S}_1	\mathbf{I}_3	NO: $z(\mathbf{I}_2) > z(\mathbf{I}_3) > z(\mathbf{I}_4)$
\mathbf{S}_2	\mathbf{I}_4	YES: $z(\mathbf{I}_3) > z(\mathbf{I}_4) < z(\mathbf{I}_5)$
\mathbf{S}_4	\mathbf{I}_2	NO: $z(\mathbf{I}_1) > z(\mathbf{I}_2) > z(\mathbf{I}_3)$
\mathbf{S}_6	\mathbf{I}_5	NO
\mathbf{S}_9	\mathbf{I}_1	NO

Table 1: Check for requirement (iii) in the definition of snout vertices.

Hence, the only snout at level k in this part of the glacier is vertex \mathbf{S}_2 . As input sites are iteratively removed from the glacier’s outline in the DCE process, the combination of requirements allows a robust identification of convex portions of the boundary that point downslope, i.e. glacier tongues/snouts. Finally, skeleton stretches which satisfy requirements (i) and (ii) but not requirement (iii) are further removed.

Hence, we obtain a snout hierarchy tied to the edge hierarchy: with a single threshold (the level $k = f(A)$ of the DCE), we can extract both a set of skeletal edges and a set of snouts for a given continuous ice body of area A .

4.3. Definition of skeleton waypoints

Let us have a closer look at the final pruned skeleton in Figure 10. The solid black lines are the remaining edges while the black dots are just a subset of the vertices in the pruned skeleton that we downsampled for simplicity (these vertices are *waypoints* distant from at least 1000 m). Clearly the skeleton edges are far from a set of flowlines, except maybe in the ablation area. The location of glacier heads and snouts looks satisfying but major flaws appear:

- many edges in the skeleton significantly deviate from the local steepest slope direction, i.e. do not at all cross elevation contours at a right angle,
- the skeleton has cycles (around inner rocks).

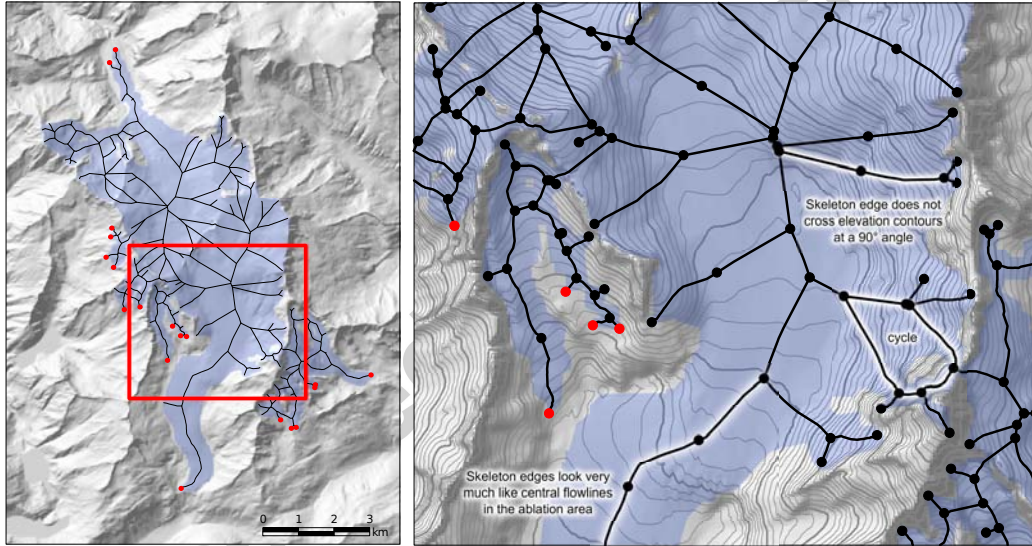


Figure 10: Example of flaws in the pruned skeletal graph, notably the deviation of skeleton edges from steepest slope directions and the presence of cycles. Black dots are a downsampled subset of skeleton vertices (waypoints), and red dots are snout vertices.

We will see that we can build another graph which links those same skeleton vertices/waypoints, but which do not exhibit these flaws, provided we can *quantify* what a ‘significant deviation from the local steepest slope direction’ is.

276 5. Construction of optimum branchings

277 In this section we define a *cost function* that will allow us to rate how
 278 much an edge between two vertices deviates from a slope line, and to select
 279 a suitable set of edges.

280 5.1. Rationale

281 Douglas (1994) recalls that computing the least-cost path (with respect
 282 to various factors such as slope, soil cover, etc.) between a point A and a
 283 point B involves three steps:

- 284 1. the definition of a *cost of movement* for an elementary movement from
 285 A to A' (close to A);
- 286 2. the computation of the *accumulated cost surface* spreading from the
 287 starting point, that sums the costs of all elementary movements;
- 288 3. the construction of the least-cost path as the *slope line* of the accumu-
 289 lated cost surface starting at B and ending at A (Warntz, 1957).

290 If we want a least-cost path to look like a steepest ascent or descent line,
 291 we can figure out what the corresponding cost function has to look like by
 292 reversing the three steps:

- 293 3. The least-cost path has to look like a topographical slope line (it will
 294 never be a true one though, unless B is strictly upslope or downslope
 295 from A)
- 296 2. This implies that the *accumulated cost surface* has to 'look like' the
 297 topographical surface z around A;
- 298 1. It means that the local *cost of movement* has to 'look like' a *differential*
 299 of the topographical surface, i.e. depend on its gradient ∇z .

300 The next section presents a cost function designed according to this ra-
 301 tionale.

302 5.2. Definition of the cost function

303 Consider an elementary displacement $\delta \mathbf{x} = (dx, dy)$ from $\mathbf{x} = (x, y)$ to
 304 $\mathbf{x}' = (x', y') = \mathbf{x} + \delta \mathbf{x} = (x + dx, y + dy)$. The cost of this elementary
 305 displacement will be defined as:

$$\begin{aligned}
 C_{\uparrow}(\mathbf{x}, \mathbf{x} + \delta\mathbf{x}) &= [z_{\max} - z(\mathbf{x})] - [z(\mathbf{x} + \delta\mathbf{x}) - z(\mathbf{x})] + \lambda\|\delta\mathbf{x}\| \\
 &= \underbrace{\|\nabla z\|\|\delta\mathbf{x}\|}_{(1)} - \underbrace{(\nabla z) \cdot \delta\mathbf{x}}_{(2)} + \underbrace{\lambda\|\delta\mathbf{x}\|}_{(3)}
 \end{aligned}$$

306 where $\|\delta\mathbf{x}\| = \sqrt{dx^2 + dy^2}$ is the length of the displacement, ∇z is the
 307 gradient vector of the topographic surface at point \mathbf{x} , and λ is a friction factor
 308 (scalar) in $\text{m} \cdot \text{m}^{-1}$. This cost is expressed in meters of potential energy and
 309 is the sum of three terms:

- 310 (1) is the maximum elevation (relative to $z(\mathbf{x})$) we could reach with a
 311 displacement of length $\|\delta\mathbf{x}\|$ starting at \mathbf{x} . By definition of the gradient,
 312 this maximum elevation is $z_{\max} = \|\nabla z\|\|\delta\mathbf{x}\|$, which is always positive.
- 313 (2) is the elevation we actually reached with the displacement $\delta\mathbf{x}$, which
 314 is $z' = (\nabla z) \cdot \delta\mathbf{x}$ (note that z' is algebraic and may be negative).
 315 Consequently, the difference (1) – (2), which is always positive whatever
 316 the displacement, is a measure of *how much higher* we could have gotten
 317 with a displacement of the same length. If the displacement is in the
 318 direction of the gradient (i.e. upslope) then ∇z and $\delta\mathbf{x}$ are colinear
 319 and $(\nabla z) \cdot \delta\mathbf{x} = \|\nabla z\|\|\delta\mathbf{x}\|$. Hence (1) and (2) cancel out in the
 320 case of a steepest *ascent*: the cost will be low. Conversely, if we move
 321 downslope, $(\nabla z) \cdot \delta\mathbf{x}$ is negative and (1) – (2) is largely positive: the
 322 displacement is very costly.
- 323 (3) is a friction term stabilizing the cost function: whatever the direction
 324 (upslope, downslope or along an elevation contour), there is always a
 325 cost λ for moving 1 meter across the surface. The effect is to smooth
 326 trajectories and to prevent paths from following too closely the small-
 327 scale irregularities on the surface.

328 We call C_{\uparrow} the *upslope* cost function, which is obviously not symmetric:

$$C_{\uparrow}(\mathbf{x}, \mathbf{x}') \neq C_{\uparrow}(\mathbf{x}', \mathbf{x})$$

329 The definition of C_{\uparrow} looks unusual, as classical cost functions (see e.g.
 330 Kienholz *et al.*, 2014) are simply the product of a scalar impedance $I(\mathbf{x})$
 331 by the length of the elementary displacement: $C(\mathbf{x}, \mathbf{x} + \delta\mathbf{x}) = I(\mathbf{x})\|\delta\mathbf{x}\|$.

Hence, every displacement of length $\|\delta\mathbf{x}\|$ around \mathbf{x} has the same cost whatever the direction (C is necessarily isotropic). This kind of formulation is easily solved in classical GIS softwares (it only requires to specify the impedance raster, and the start and end points). However, we believe that our formulation is preferable for steepest ascent/descent problems, which are anisotropic in nature (see also Collischonn and Pilar, 2000).

338

339 Similarly, we can define a *downslope* cost function:

$$C_{\downarrow}(\mathbf{x}, \mathbf{x} + \delta\mathbf{x}) = \underbrace{+(\nabla z) \cdot \delta\mathbf{x}}_{(1)} - \underbrace{(-\|\nabla z\|\|\delta\mathbf{x}\|)}_{(2)} + \underbrace{\lambda\|\delta\mathbf{x}\|}_{(3)}$$

This time, (2) is the *minimum* elevation we could reach with a displacement of length $\|\delta\mathbf{x}\|$. The difference (1) – (2) is always positive and is a measure of *how much lower* we could have gotten with a displacement of the same length: (1) and (2) cancel out in the case of a steepest *descent*. Conversely, if we move upslope, (1) – (2) is large and the cost is high.

345

346 Finally, these cost functions satisfy the requirement that the steepest ascent path from \mathbf{x} to \mathbf{x}' is also the steepest descent path from \mathbf{x}' to \mathbf{x} (assuming the same friction factor λ):

$$C_{\uparrow}(\mathbf{x}, \mathbf{x}') = C_{\downarrow}(\mathbf{x}', \mathbf{x})$$

In the following, we only use the upslope cost function C_{\uparrow} ; we will see why it is more convenient to treat the problem from downslope up. Moreover, in order to improve flow convergence near the glacier boundary, we slightly modify the cost function by increasing the friction factor λ near the boundary (this will penalize flowlines wandering along the boundary):

$$C_{\uparrow}(\mathbf{x}, \mathbf{x} + \delta\mathbf{x}) = \|\nabla z\|\|\delta\mathbf{x}\| - (\nabla z) \cdot \delta\mathbf{x} + \underbrace{\left(\lambda_{\infty} + (\lambda_0 - \lambda_{\infty})e^{-\frac{D(\mathbf{x})}{D_{\lambda}}} \right)}_{\lambda(\mathbf{x})} \|\delta\mathbf{x}\|$$

where $D(\mathbf{x})$ is the distance to the boundary at point \mathbf{x} , λ_{∞} is the friction cost far from the boundary, $\lambda_0 > \lambda_{\infty}$ is the friction cost at the boundary and D_{λ} is the scale of decrease with distance. Note that this modified cost is still

354

355

356

357 anisotropic: $\lambda(\mathbf{x})$ is an impedance, but it is not the dominant term of the
 358 cost function. The values $\lambda_\infty = 0.035 \text{ m} \cdot \text{m}^{-1}$, $\lambda_0 = 5\lambda_\infty = 0.175 \text{ m} \cdot \text{m}^{-1}$,
 359 and $D_\lambda = 150 \text{ m}$ were found to give very good results on all glaciers.

360

361 Finally, since we use a raster DEM (i.e. a square lattice with only 8
 362 possible elementary displacements from a given grid point $\mathbf{x}_{i,j}$), we define a
 363 discrete version of C_\uparrow :

$$C_\uparrow(\mathbf{x}_{i,j}, \mathbf{x}_{i+\delta i, j+\delta j}) = \left(z_{i,j} + s_{\max} \sqrt{\delta i^2 + \delta j^2} \right) - z_{i+\delta i, j+\delta j} + \lambda(\mathbf{x}_{i,j}) \sqrt{\delta i^2 + \delta j^2}$$

364 where

$$s_{\max} = \max_{0 < (\delta i^2 + \delta j^2) \leq 2} \left\{ \frac{z_{i+\delta i, j+\delta j} - z_{i,j}}{\sqrt{\delta i^2 + \delta j^2}} \right\}$$

365 is the estimated upward slope (norm of the gradient) at pixel $\mathbf{x}_{i,j}$. If the
 366 above expression for s_{\max} is negative, it is of course set to zero: there is a
 367 local maximum at $\mathbf{x}_{i,j}$.

368 5.3. Cost assignment for paths between waypoints

369 We use Dijkstra's algorithm (Dijkstra, 1959) to compute the least-cost
 370 path between each pair of waypoints. It uses the elementary cost function
 371 to produce an accumulated cost surface spreading around a start point \mathbf{S} ,
 372 and a backlink grid which gives the direction *opposite* to the gradient of the
 373 accumulated cost surface at each pixel. The least-cost path from \mathbf{S} to any
 374 point is constructed in the reverse direction, starting from the destination and
 375 following the backlinks to \mathbf{S} . In our case, the cost is defined from downslope
 376 up, so a backlink is defined from upslope down (see Figure 11).

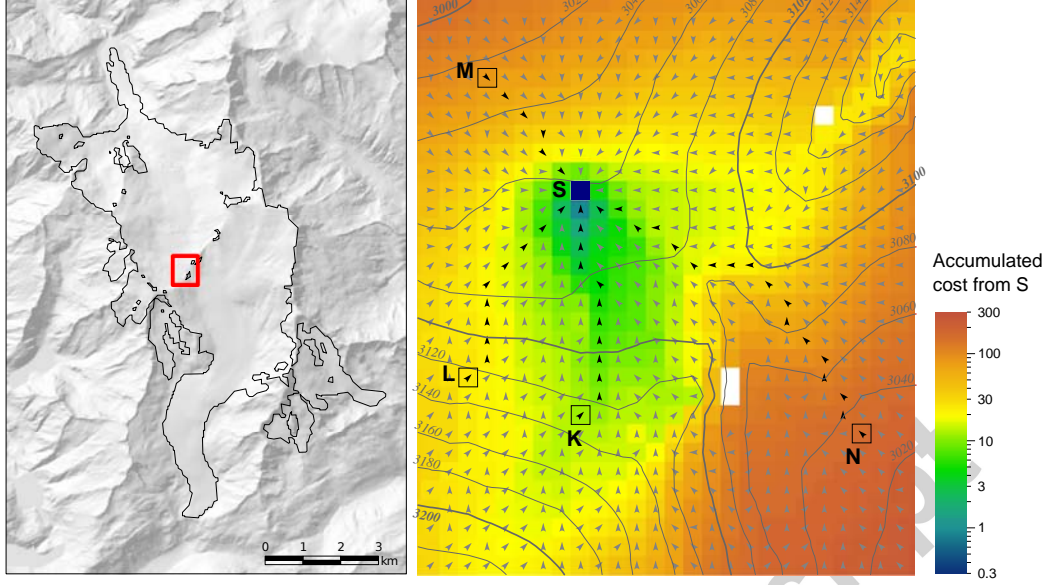


Figure 11: Example of accumulated cost surface, spreading from a start point **S**. Arrows indicate the backlinks: the least-cost path from **S** to any destination (**K**, **L**, **M**, **N**, etc.) is constructed from the destination to the start **S**, following the backlink grid. White pixels are ice-free zones (inner rocks) across which no displacement is possible.

Figure 11 illustrates the effects of the definition of C_{\uparrow} :

- destination **K** is located right upslope from start **S**, at an elevation of about 3130 m. Since edge (**S**,**K**) is almost a steepest ascent path, its cost is low: $C_{\uparrow}(\mathbf{S}, \mathbf{K}) = 11.2$
- destination **L** is located at about the same elevation, but one has to cross elevation contours at some angle to get there from **S**. The cost is higher: $C_{\uparrow}(\mathbf{S}, \mathbf{L}) = 25.3$
- destination **M** is located at an elevation lower than **S**, about 3030 m. Consequently, the edge from **S** to **M** is far from a steepest *ascent* (it is almost a steepest *descent*), and has a high cost: $C_{\uparrow}(\mathbf{S}, \mathbf{M}) = 80.5$ (note that this path would in contrary have a very low cost with respect to the downslope cost function C_{\downarrow})
- finally, destination **N** is located on the other side of a ridge. In order to reach **N** from **S**, one must first climb to a pass at about 3100 m (low cost), but then go down (high cost). We have $C_{\uparrow}(\mathbf{S}, \mathbf{N}) = 169.3$

392 We use this algorithm to compute the costs between any pair of skeletal
 393 vertices/waypoints. In practice, we only compute the costs to the n nearest
 394 neighbors of each vertex with respect to the cost function, using a local run
 395 of Dijkstra’s algorithm that is aborted as soon as n neighbor vertices have
 396 been visited (straightforward with an implementation based on a priority
 397 queue). The value $n = 30$ turned out to be largely sufficient for the following
 398 steps. We obtain the kind of graph shown in Figure 12. Each edge can be
 399 traversed in both directions, but at a different cost in each direction: the
 400 graph is *directed*.

401 5.4. Identification of minimum spanning branchings

402 The creation of a dense, redundant graph between the skeletal waypoints
 403 looks like a step backwards, compared to the simplicity of the skeleton. How-
 404 ever, graph theory provides powerful tools which will help simplify this graph
 405 again, in the way we want.

406
 407 Each waypoint (vertex) has several incoming and outgoing edges in the
 408 new directed graph. The set of flowlines we are looking for is a *branching* or,
 409 synonymously, a *directed spanning tree* i.e. a graph \mathcal{T} such that:

- 410 • \mathcal{T} contains no cycle,
- 411 • each vertex has *one and only one* incoming edge: each vertex is visited
 412 (the tree is *spanning*), but no two edges of \mathcal{T} enter the same vertex
 413 (i.e., each vertex has only one downstream pixel, since we build the
 414 flowlines from downstream towards upstream).

415 Of course, such a tree \mathcal{T} has to be rooted at a snout, i.e. a special vertex
 416 without an incoming edge. Moreover, we want the edges of this tree to be
 417 —as much as possible— steepest climb routes, i.e. to have low costs with re-
 418 spect to our cost function. Extracting a subset of edges (a subgraph) which
 419 satisfies all these requirements (being a tree, being spanning, and having
 420 a minimal cost) is a classical problem called Directed Minimum Spanning
 421 Tree (DMST) extraction. It is efficiently solved with the Chu-Liu/Edmonds
 422 algorithm (Chu and Liu, 1965; Edmonds, 1967): in this study we use the
 423 implementation of Tofigh (2009), based on the Boost Graph Library (Siek et
 424 al., 2002).

425

426 Since there are several snouts in a glacier complex, the subgraph may
427 actually be a *forest* i.e. a set of trees, each one rooted at a different snout.
428 The single-root version of the Edmonds algorithm is easily extended to the
429 multiple-root case: a virtual ‘master’ root is created, and zero-cost edges are
430 added from this root to each snout (see Figure 12).

431

432 Figure 13 shows the output of the algorithm for the Rhone-Trift glacier
433 complex. It is worth noting that the segmentation of the complex into in-
434 dividual glaciers is a by-product of the method: each snout ‘drains’ a set of
435 upstream vertices which form its catchment.

436

Accepted manuscript

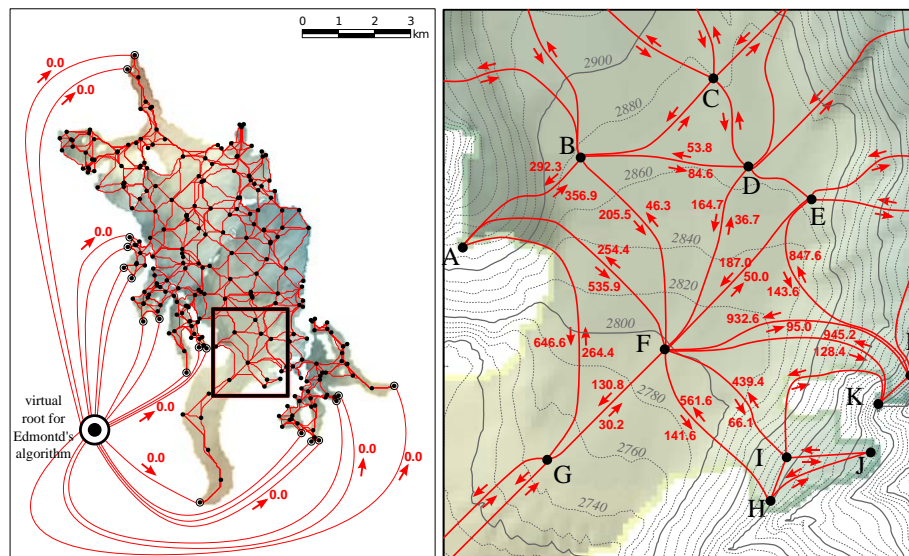


Figure 12: Edges and associated costs between skeleton waypoints in the Rhone-Trift glacier complex. Left: example of initial graph with numerous edges linking pairs of waypoints. For clarity, the plot displays only the edges between natural (planar) neighbors but a much denser graph can be created. Right: zoom on a region. Figures in red are the costs of each edge, in both directions.

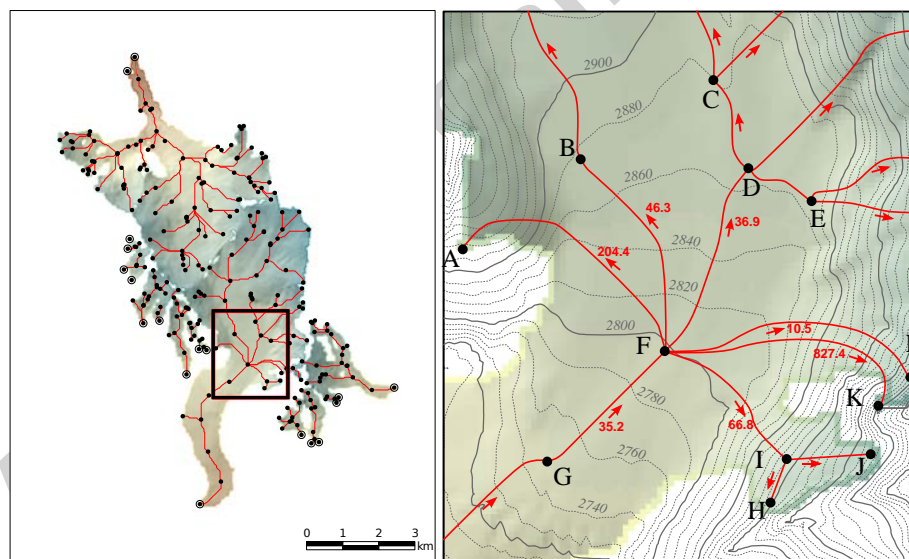


Figure 13: Output of the Chu-Liu/Edmonds algorithm with the set of edges and costs of Figure 12. The minimum branching (Directed Minimum Spanning Tree/Forest) allows to visit all waypoints, starting from a snout and always moving as upslope as possible.

Figure 14 is a zoom on a pass across the topographical divide between Rhone and Trift glaciers (Undri Triftlimi). It explains why no edge in the DMST/DMSF should cross any major topographical ridge. Let us suppose that the ridge-crossing edge (\mathbf{K}, \mathbf{L}) is part of the DMSF, denoted \mathcal{F} and of total cost $C_{\uparrow}(\mathcal{F})$. In this case, point \mathbf{L} ultimately drains to Trift glacier's snout. However, the other incoming edge to \mathbf{L} , (\mathbf{M}, \mathbf{L}) , has a lower cost than (\mathbf{K}, \mathbf{L}) : hence if we remove (\mathbf{K}, \mathbf{L}) from \mathcal{F} and add (\mathbf{M}, \mathbf{L}) , we obtain a forest \mathcal{F}' that is still spanning (\mathbf{L} is visited i.e. has an incoming edge) and has a lower total cost $C_{\uparrow}(\mathcal{F}') = C_{\uparrow}(\mathcal{F}) + C_{\uparrow}(\mathbf{M}, \mathbf{L}) - C_{\uparrow}(\mathbf{K}, \mathbf{L}) < C_{\uparrow}(\mathcal{F})$. This means that \mathcal{F} was not a DMSF in the first place (it is spanning but not of minimum cost): point \mathbf{L} has to flow to Rhone glacier's snout, and no edge should go through the pass. Hence, our procedure is efficient not only for flowline extraction, but also for glacier segmentation.

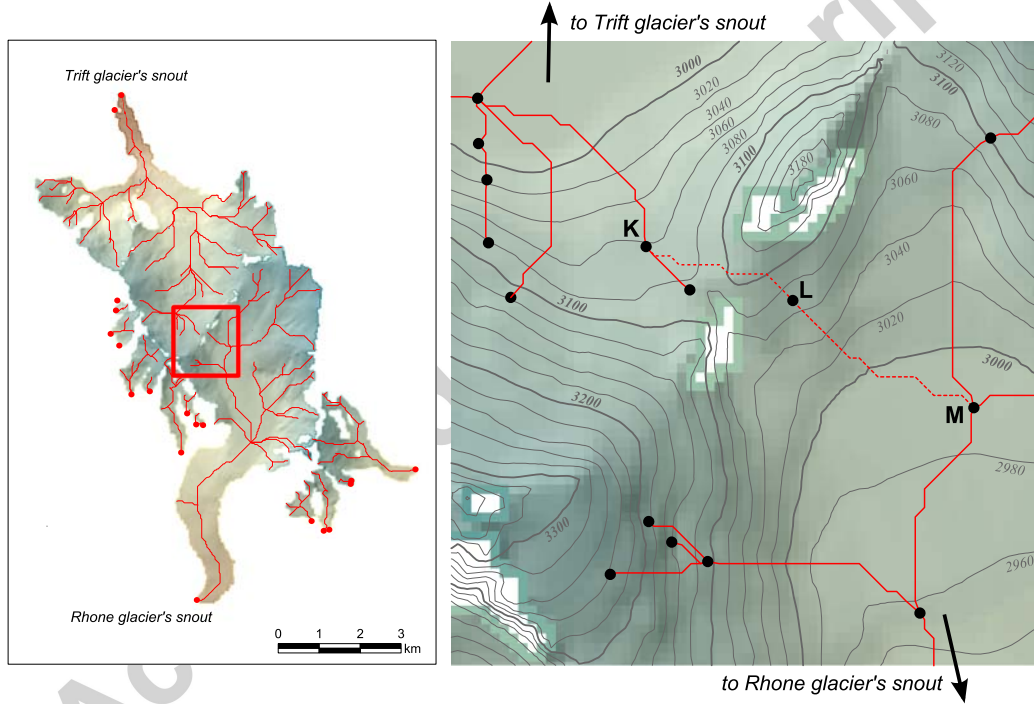


Figure 14: Zoom on the minimum branching in the vicinity of Undri Triftlimi, a pass on the divide between Rhone and Trift glaciers. Vertex \mathbf{L} , which is located south of the ridge, has to be visited from \mathbf{M} and not from \mathbf{K} in the Directed Minimum Spanning Tree/Forest: no edge should go across any major divide.

6. Conclusion and perspectives

In this paper we proposed a new method to extract glacier flowlines, based on Voronoi skeletonization of glacier boundaries, skeleton pruning using Discrete Curve Evolution (DCE), and the construction of a Directed Minimum Spanning Tree between skeletal vertices with respect to an anisotropic, up-slope cost function C_{\uparrow} .

The application of the method requires limited parameter tweaking: it only requires a selection rule $k = f(A)$ for the level k of the DCE as a function of glacier area A (2 parameters), and 3 parameters for the friction law (i.e. the isotropic term of the cost function). Table 2 sums up the values used on the whole domain of Figure 2a (1200 km² of glaciers, the largest contiguous icefield having an area of 261 km²).

DCE level selection $k = 2 + \lfloor k_0 A^\gamma \rfloor$	k_0	13.5
	γ	0.8
Cost function $C_{\uparrow}(\mathbf{x}, \mathbf{x} + \delta\mathbf{x}) = \ \nabla z\ \ \delta\mathbf{x}\ - (\nabla z) \cdot \delta\mathbf{x} + \lambda(\mathbf{x}) \ \delta\mathbf{x}\ $ with $\lambda(\mathbf{x}) = \lambda_{\infty} + (\lambda_0 - \lambda_{\infty}) e^{-\frac{D(\mathbf{x})}{D_{\lambda}}}$	λ_{∞}	0.035 m · m ⁻¹
	λ_0	0.175 m · m ⁻¹
	D_{λ}	150 m

Table 2: Parameters of the method.

The method currently lacks a quality assessment, though this could be done on a small subset of glaciers by comparison with manually-extracted flowlines. The large-scale visual assessment is however very satisfying, and the resulting network can be used to compute indices such as Strahler orders, bifurcation ratios, etc. Many scaling properties of glaciers, such as volume-area scaling (Bahr et al., 1997) or power-law behavior of accumulation basin areas (Gsell et al., 2014), originate in glacier branching topology: such properties could act as a ‘lever arm’ for tackling the problem of catchment-scale glacier flow dynamics, much like other fundamental symmetries (plane-strain or radial), as advocated by Bahr and Peckham (1996). We hope that this study will foster ideas in this field.

7. Acknowledgments

This work has been supported by an EC2CO grant from the French CNRS (INSU). The authors acknowledge the Swiss Federal Office of Topography (SwissTopo) for providing the 25-meter DEM.

8. References

- [1] Arendt, A., Bolch, T., Cogley, J. G., Gardner, A., Hagen, J. O., Hock, R., Kaser, G., et al., 2012. Randolph Glacier Inventory – A Dataset of Global Glacier Outlines: Version 3.2. Global Land Ice Measurements from Space, Boulder, CO, USA. Digital Media.
URL <http://www.glims.org/RGI/>
- [2] Bahr, D. B., Meier, M., Peckham, S. D., 1997. The physical basis of glacier volume-area scaling. *J. Geophys. Res.* 102, 20355–20362.
- [3] Bahr, D. B., Peckham, S. D., 1996. Observations and analysis of self-similar branching topology in glacier networks. *J. Geophys. Res.* 101, 25511–25521.
- [4] Bai, X., Latecki, L. J., Liu, W.-Y., 2007. Skeleton pruning by contour partitioning with discrete curve evolution. *IEEE Trans. Pattern Anal. Mach. Intell.* 29 (3), 449–462.
- [5] Barber, C. B., Dobkin, D. P., Huhdanpaa, H. T., 1996. The Quickhull algorithm for convex hulls. *ACM Trans. on Mathematical Software* 22 (2), 469–483.
URL <http://www.qhull.org>
- [6] Blum, H., 1967. A Transformation for Extracting New Descriptors of Shape. In: Wathen-Dunn, W. (Ed.), *Models for the Perception of Speech and Visual Form*. MIT Press, Cambridge, pp. 362–380.
- [7] Brandt, J. W., Algazi, V. R., 1992. Continuous skeleton computation by Voronoi diagram. *CVGIP: Image Understanding* 55 (3), 329–338.
- [8] Chu, Y. J., Liu, T. H., 1965. On the shortest arborescence of a directed graph. *Science Sinica* 14, 1396–1400.
- [9] Collischonn, W., Pilar, J. V., 2000. A direction dependent least-cost-path algorithm for roads and canals. *International Journal of Geographical Information Science* 14 (4), 397–406.
- [10] Dijkstra, E. W., 1959. A note on two problems in connexion with graphs. *Numerische Mathematik* 1, 269–271.
URL <http://dx.doi.org/10.1007/BF01386390>

- 509 [11] Douglas, D. H., 1994. Least-cost Path in GIS Using an Accumulated
510 Cost Surface and Slopelines. *Cartographica* 31 (3), 37–51.
- 511 [12] Edmonds, J., 1967. Optimum branchings. *J. Res. Natl. Bur. Stand.* 71B,
512 233–240.
- 513 [13] Garbrecht, J., Martz, L. W., 1997. The assignment of drainage direction
514 over flat surfaces in raster digital elevation models. *Journal of Hydrology*
515 193 (1-4), 204–213.
- 516 [14] Gsell, P.-S., Le Moine, N., Moussa, R., Ribstein, P., 2014. Identifying
517 the probabilistic structure of drained areas as a function of hypsometry
518 in river networks. *Hydrological Processes*.
519 URL <http://dx.doi.org/10.1002/hyp.10296>
- 520 [15] Gupta, V. K., Waymire, E., Wang, C. T., 1980. A representation of an
521 instantaneous unit hydrograph from geomorphology. *Wat. Resour. Res.*
522 16 (5), 855–862.
- 523 [16] Kienholz, C., Rich, J. L., Arendt, A. A., Hock, R., 2014. A new method
524 for deriving glacier centerlines applied to glaciers in Alaska and north-
525 west Canada. *The Cryosphere* 8 (2), 503–519.
- 526 [17] Latecki, L. J., Lakämper, R., 2002. Application of Planar Shape Com-
527 parison to Object Retrieval in Image Databases. *Pattern Recognition*
528 35, 15–29.
- 529 [18] Le Bris, R., Paul, F., 2013. An automatic method to create flow lines
530 for determination of glacier length: A pilot study with Alaskan glaciers.
531 *Computers & Geosciences* 52, 234–245.
- 532 [19] Le Moine, N., 2013. CLaRiNet: Catchment, Landform, and River Net-
533 work analysis – A geomorphological toolbox for Scilab, User Manual
534 (draft version). UPMC.
535 URL <http://www.sisyphe.upmc.fr/~lemoine/resources.htm>
- 536 [20] Machguth, H., Huss, M., 2014. The length of the world’s glaciers – a
537 new approach for the global calculations of center lines. *The Cryosphere*
538 8, 1741–1755.

- 539 [21] Martz, L. W., Garbrecht, J., 1998. The treatment of flat areas and
 540 depressions in automated drainage analysis of raster digital elevation
 541 models. *Hydrological Processes* 12 (6), 843–855.
- 542 [22] Rodríguez-Iturbe, I., Valdés, J. B., 1979. The geomorphological struc-
 543 ture of the hydrologic response. *Wat. Resour. Res.* 15, 1409–1420.
- 544 [23] Scilab Enterprises, 2012. Scilab: Free and Open Source software for
 545 numerical computation. Scilab Enterprises, Orsay, France.
 546 URL <http://www.scilab.org>
- 547 [24] Siek, J. G., Lee, L.-Q., Lumsdaine, A., 2002. The Boost Graph Li-
 548 brary: User Guide and Reference Manual. Addison-Wesley, Boston,
 549 Massachusetts.
 550 URL <http://www.boost.org/doc/libs/release/libs/graph/>
- 551 [25] SwissTopo, 2004. DHM25, The digital height model of Switzerland,
 552 Product Information. Federal Office of Topography, Wabern, CH.
- 553 [26] Tofigh, A., 2009. Optimum Branchings and Spanning Arborescences.
 554 Accessed on SourceForge.
 555 URL <http://sourceforge.net/projects/edmonds-alg/>
- 556 [27] Warntz, W., 1957. Transportation, social physics, and the law of refrac-
 557 tion. *The Professional Geographer* 9 (4), 2–7.
 558 URL http://dx.doi.org/10.1111/j.0033-0124.1957.094_2.x